Crystal Growth of Novel 3D Skeleton Uranyl Germanium Complexes: Influence of Synthetic Conditions to Crystal Structures

Haijian Li[†,‡,*], Philip Kegler[‡], Evgeny V. Alekseev[‡,§,*]

[†]Science and Technology on Combustion and Explosion Laboratory, Xi'an Modern Chemistry Research Institute, Xi'an 710065, China

[‡]Institute of Energy and Climate Research (IEK-6), Forschungszentrum Jülich GmbH , 52428 Jülich, Germany

[§]Institut für Kristallographie, RWTH Aachen University, 52066 Aachen, Germany

contact E-Mail: h.j.li@outlook.com,e.alekseev@fz-juelich.de

ABSTRACT:

Five centrosymmetric uranyl germanate compounds, $K_8BrF(UO_2)_3(Ge_2O_7)_2$,$Rb_6(UO_2)_3(Ge_2O_7)_2{\cdot}0.5H_2O$, $Cs_6(UO_2)_2Ge_8O_{21}$ and $\boldsymbol{A}^+_2(UO_2)_3(GeO_4)_2$ ($\boldsymbol{A}^+$=Rb^+, Cs^+), were synthesized in the work. $K_8BrF(UO_2)_3(Ge_2O_7)_2$and $Rb_6(UO_2)_3(Ge_2O_7)_2{\cdot}0.5H_2O$ were obtained from mixed KF–KBr fluxand hydrothermal condition, respectively. Both structures crystallized in triclinic ***P***-1 space group and have similar anionic frameworks featured by novel hexagon shaped12-membered channels. The condensation of two different types of SBUs [UGe_4] pentamers (**A**) and (**A2**) results in the formations of $K_8BrF(UO_2)_3(Ge_2O_7)_2$ and $Rb_6(UO_2)_3(Ge_2O_7)_2{\cdot}0.5H_2O$ frameworks. $Cs_6(UO_2)_2Ge_8O_{21}$ was obtained from CsF–CsCl high temperature flux, and it also crystallized in centrosymmetric triclinic***P***-1 space group. The structure of $Cs_6(UO_2)_2Ge_8O_{21}$ exhibited a novel oxo-germanate layer which based upon germanate tetrahedra and trigonal bipyramids. Two new SBUstypes, (**$4^2.5^2$-A2**) and (**5^4-A2**)[UGe_4] pentamers, were found in the structure of $Cs_6(UO_2)_2Ge_8O_{21}$. $\boldsymbol{A}^+_2(UO_2)_3(GeO_4)_2$ ($\boldsymbol{A}^+$=Rb^+, Cs^+) were synthesized by high temperature/high pressure (HT/HP) technique, and both structures with oval-shaped 12-membered channels crystallized in centrosymmetric orthorhombic ***P***nma space group. The extreme condition led to the formation of [U_2Ge_2] tetramers (**E**), which consists of 7-coordinated U and 5-coordinated Ge. Different synthetic methods of uranyl germanate compounds resulted in distinct coordination environment of uranyl cations and variety of U=O and U–O bond lengths, further affecting the dimensionality and types of uranyl units and SBUs.The Raman and IR- spectra of five new phases were collected and analyzed.

1. INTRODUCTION

Recently, salt-inclusion uranyl silicate and germanatephases have been synthesized by flux growth method, and these compounds exhibit rich and complex micro-porous structures. For example, one of the typical frameworks,$\boldsymbol{A}^{6+}(UO_2)_3(\boldsymbol{T}_2O_7)_2$($\boldsymbol{A}$=salt-inclusion units, $\boldsymbol{T}$ =Si, Ge) with 12-membered channels crystallizing in orthorhombic system.[1-3] It is based upon UO_6 tetragonal bipyramids and pyro-silicate/germanate (Si_2O_7, Ge_2O_7) units, and the salt inclusion lattices including the alkali-metal cations and halides anions reside within the channels. In the class of U−Si−O phases, the structure of $K_8(K_5F)U_6Si_8O_{40}$ can be constructed by the combination of two typical slabs and the salt-inclusion units (K_5F) which is located within the complex framework with 10-membered rings.[4] Morrison et al. found that the controllable synthesis of salt-inclusion compounds could beachieved using enhanced flux crystal growth method.[5] The diverse salt-inclusions such as [Cs_3F], [Cs_5F], [Cs_6Cl] units were able to fit into the large voids of the 3D uranyl silicate structures. In contrast to silicates, germanate compounds have lager volume of pores or channels, which may accommodate different and potentially more complex salt inclusion units.[3,6-8]

In recent studies, uranyl oxo-anioncomplexes with diverse open-framework structures have been well explored. For example, in uranyl silicates family,corner-sharing condensation of silicate tetrahedra leads to formation of Si_2O_7 pyro-silicates, Si_4O_{12} square, Si_4O_{13} 0-D chain, Si_8O_{22} cluster, Si_2O_6 and Si_6O_{17} unbranched chains, Si_4O_{10} tubular and multiple chains, Si_8O_{20} and $Si_{12}O_{33}$ column, $Si_4O_{10}$and Si_5O_{13}sheets, Si_8O_{19} double sheetand $Si_{10}O_{22}$ slab.[4,5,9-16]Additionally, some compounds exhibit a combination of several silicate motifs for example $K_{14}(UO_2)_3Si_{10}O_{30}$ containing Si_6O_{16} chains and Si_2O_7 groups.[9]Compared to silicates, germanium can bond different number of O atoms to form 4-, 5- and 6-coordinated polyhedra at ambient

conditions.[17-19] The diversity of coordination environments provides more possibilities for the formation of complex and flexible uranyl oxo-germanate frameworks. Among the known uranium germanates, the 3D framework of only one uranyl compound, $Ag_2(UO_2)_3(GeO_4)_2(H_2O)_2$,contains5-fold coordinated germanates (triangular bipyramids).[20]Additionally, the U−Ge−O systemdemonstratesuch structural features as cation-cation interaction of uranyl groups[21] and extra-large pore structures.[22]Using HT/HP hydrothermal method, Lii et al. synthesized several mixed valence U(IV)/(V)[23,24] and U(V,VI)[25,26] germanates.

Different synthetic techniques such as slow evaporation, hydrothermal, high temperature flux, high temperature/high pressure (HT/HP) solid state and HT/HP hydrothermal reactions have been widely applied for exploration of novel inorganic solid-statematerialswith actinides.Among them, high pressure synthesis not only changes structure of materials but also enables mixed-valence chemistry and rich coordination environments of actinide elements.[27,28] Our group focus on the synthesis and characterization of actinide oxo-anion and oxidic materials using different synthetic approaches especially high temperature and HT/HP technique, which is necessary for study crystal-chemical trends in these materials. A series of U/Th oxo-compounds containing borates (BO_3/BO_4),[29,30] arsenates (AsO_3 and AsO_4),[31,32]tellurites and tellurates($Te^{IV}O_3$, $Te^{IV}O_4$, and $Te^{VI}O_6$)[33,34] oxo-anions have been synthesized under extreme condition and structurally and spectroscopically characterized.

In this work, five novel uranyl germanate compounds have been synthesized and structurally characterized using single crystal X-ray diffraction, Raman and FTIR spectra. $K_8BrF(UO_2)_3(Ge_2O_7)_2$have been synthesized by high temperature flux method, and its framework is similar to that of we found in new $Rb_6(UO_2)_3(Ge_2O_7)_2{\cdot}0.5H_2O$ which was obtained

under hydrothermal condition. $Cs_6(UO_2)_2Ge_8O_{21}$have been synthesized by high temperature flux growth method,and its structure contains 4- and 5-coordinated germanium sites.$\boldsymbol{A}^+_2(UO_2)_3(GeO_4)_2$ ($\boldsymbol{A}^+$=Rb^+, Cs^+) have been prepared by HT/HP reaction. Influence of synthetic conditions on structures of the studied U−Ge−O materials has been discussed.

2. EXPERIMENTAL SECTION

Caution! *Radioactive materials such as uranium nitrate were applied for this study. All experiments in the works must be carried out under the standard radiation protection precautions.*

2.1 Crystal Growth

$K_8BrF(UO_2)_3(Ge_2O_7)_2$. Crystals of $K_8BrF(UO_2)_3(Ge_2O_7)_2$ have been obtained from mixed salts KF–KBr high temperature flux reaction. UO_3 was prepared by heating $UO_2(NO_3)_2{\cdot}6H_2O$ (International Bioanalytical Industries, Inc.) at 450° for 4h in air. A mixture of 30 mg UO_3, 22 mg GeO_2(Alfa Aesar, 99.999%), 121.9 mg KF (Alfa Aesar, 99%) and 249.6 mg KBr (Alfa Aesar, 99+%) (molar ratio U/Ge/KF/KBr = 1/2/20/20) was ground in an agate mortar, and then the mixture was loaded into a platinum crucible and heated to 700 °C for 12h, and then cooled slowly to 500°C at a rate of 5°C/h. Finally, the furnace was shut down. Green crystals of $K_8BrF(UO_2)_3(Ge_2O_7)_2$ and U_3O_8 were identified from PXRD study to be the major reaction products.

$Rb_6(UO_2)_3(Ge_2O_7)_2{\cdot}0.5H_2O$. Crystals of $Rb_6(UO_2)_3(Ge_2O_7)_2{\cdot}0.5H_2O$ were synthesized by hydrothermal method. Mixture of 100 mg $UO_2(NO_3)_2{\cdot}6H_2O$, 73.1 mg GeO_2, 907.3 mg $RbOH{\cdot}xH_2O$ (Alfa Aesar, 99%) and 9.3 mg NH_4Cl (Alfa Aesar, 98%) and 1 mL H_2O (molar ratio U/Ge/Rb/NH_4Cl = 2.28/8/90/2) was stirred in the 23 mL Teflon-lined autoclaves for 2 hours, and then the autoclave was sealed and placed inside a program controlled furnace. The

autoclave was heated to 220 °C in 2 hours, and then held at this temperature for 24 h. After this, the furnace was cooled to 80 °C with a rate of 2°C/h and then shut down. Needle shaped green crystals of $Rb_6(UO_2)_3(Ge_2O_7)_2{\cdot}0.5H_2O$, a minor reaction product, and other phases (Rb_2UO_4 and $UO_3{\cdot}2H_2O$) were found at the bottom of the autoclave.

$Cs_6(UO_2)_2Ge_8O_{21}$. Crystals of $Cs_6(UO_2)_2Ge_8O_{21}$ was obtained from high-temperature mixed salts CsF–CsCl flux reactions. A mixture of 30 mg UO_3, 131.7 mg GeO_2 (Sigma-Aldrich, 99.998%), 318.6 mg CsF (Alfa Aesar, 99%) and 353.2 mg CsCl (Alfa Aesar, 99%) (molar ratio U/Ge/CsF/CsCl = 1/12/20/20) was placed into a platinum crucible and heated to 750 °C for 12h. The crucible was cooled slowly to 500°C at a rate of 5°C/h, and then quenched to room temperature by shutting down the furnace. The minor reaction products, green crystals of $Cs_6(UO_2)_2Ge_8O_{21}$, and unknown phases with bad quality can be found in the crucible.

$A^+_2(UO_2)_3(GeO_4)_2$ (A^+=Rb$^+$, Cs$^+$).Crystals of $Cs_2(UO_2)_3(GeO_4)_2$ were obtained by mixed fluxes of Cs_2CO_3–WO_3 under the HT/HP condition. A mixture of 50 mg $UO_2(NO_3)_2{\cdot}6H_2O$, 31.3 mg GeO_2, 81.1 mg Cs_2CO_3 (Alfa Aesar, 99%) and 28.9 mg WO_3 (Alfa Aesar, 99.8%) (molar ratio U/Ge/Cs_2CO_3/WO_3 = 4/12/10/5)was loaded into a small platinum capsule with the dimension of 4 mm. After being dried for 24 h, the capsule was sealed and embedded into MgO medium. The high-pressure experiment was performed at 3 GPa and 1200°C using the piston cylinder module (Voggenreiter LP 1000-540/50). The capsule was compressed to 3 GPa in 30 minutes, and then heated up to 1200°C in 24 minutes and keep this temperature for 3h. After this, the capsule was cooled down slowly to 700 °Cat a rate of 10°C/h, and subsequently furnace was turned off. At whole experimental process the pressure remain constant and then released. The capsule was cut off, and green column-like crystals of $Cs_2(UO_2)_3(GeO_4)_2$, a major reaction product, were found along with U_3O_8, some amorphous products and flux materials. Crystals of $Rb_2(UO_2)_3(GeO_4)_2$

were synthesized by Rb_2CO_3–WO_3 flux under the same condition with $Cs_2(UO_2)_3(GeO_4)_2$. The initial materials including 100mg $UO_2(NO_3)_2{\cdot}6H_2O$, 62.5mg GeO_2, 115mg Rb_2CO_3 (Alfa Aesar, 99%) and 57.7mg WO_3 (molar ratio U/Ge/Rb_2CO_3/WO_3 = 4/12/10/5) were used for the synthesis of $Rb_2(UO_2)_3(GeO_4)_2$. The major reaction products, $Rb_2(UO_2)_3(GeO_4)_2$, has been found in the capsule.

2.2 Powder Samples Synthesis

Pure phase of $Cs_6(UO_2)_2Ge_8O_{21}$ was prepared by high temperature solid state reaction method. $Cs_6(UO_2)_2Ge_8O_{21}$ phase was obtained at 750 °C for 24 hours. The initial chemicals including $(UO_2)(NO_3)_2(H_2O)_6$, GeO_2 and Cs_2CO_3 with a molar ratio of 2/8/3 were mixed and loaded into a ceramic crucible covered with a lid. The crucible was placed into a furnace and heated up to 750 °C at a rate of 300 °C/h, and then kept the temperature for 24h. Finally, the furnace was switched off. The obtained powder sample was grounded, and then used for the PXRD measurement.

2.3 Crystallographic Studies

The appropriate crystals for all uranyl germanates were selected for data collection and were mounted on the glass fibers. The data were collected at room temperature using a Mo Kα1 tube (λ = 0.71073 Å) that runs at 50 kV and 0.8 mA on an Agilent SuperNova diffractometer. The 3D crystallographic data for all compounds were collected using the narrow-frame method in ω-scan mode and were filtered using the CrysAlis^{Pro} software. The crystal structures of title phases are determined by the direction method of SHELXL-2018 program and the software suite WinGX v2014.1.[35]The final structures of compounds were checked by the program Addsym of

PLATON.[36] The crystallographic data and experimental conditions are given in **Table 1**. The disorder of Br^- and F^- positions within the salt-inclusion units of $K_8BrF(UO_2)_3(Ge_2O_7)_2$ resulted in the high R-values for the structural refinements. Several methods including the SXRD data collection at low temperature, variations of KF/KBr flux ratios and cooling ranges have been used for obtaining better crystals and decreasing the R-value, but the problem was not solved.

2.4 PXRD Characterization

The PXRD pattern of $Cs_6(UO_2)_2Ge_8O_{21}$ was collected by a Bruker-AXS D4 Endeavor diffractometer equipped with a copper tube. The wavelength λ is 1.54187 Å. The scanning range of measurements is from 10° to 80°. The counting time per step is 10 s. The recorded PXRD data for the pure phase was compared with the calculated patterns generated from single crystal structures, as shown in **Figure S1**.

2.5 SEM/EDS Analysis

The chemical compositions of all obtained U−Ge compounds were confirmed using a Quanta 200F scanning electron microscope equipped with an energy-dispersive spectrometer. The EDS results for the titled compounds are consistent with the chemicalcompositions obtained from SXRD, and can be seen in **Supporting Information** (**Figure S2** and **Table S1**).

2.6 Vibrational Spectroscopy

The unpolarized Raman spectra of the obtained single crystals were collected using a Horiba LabRAM HR spectrometer with a Peltier-cooled multichannel CCD detector. The incident radiation was generated by a He−Ne laser at a power of 17 mW (λ = 632.81 nm). The

spectral resolution was around 1 cm^{-1} with a slit of 100 μm. The Raman spectra of four U−Ge compounds were recorded at room temperature in the range of 100−1000 cm^{-1}, and the Raman spectra of $Rb_6(UO_2)_3(Ge_2O_7)_2{\cdot}0.5H_2O$was also collected in the range of 1000−4000 cm^{-1}.

The infrared (IR) spectra were collected at room temperature using a Bruker Equinox spectrometer. The KBr-pellet standard method was used for the preparation of the samples. The IR spectra were collected in the range from 400 to 1000 cm^{-1}.

2.7 BVS Analysis

Bond-valence sums calculation for the obtained uranyl germanate compounds was performed using Burns' parameters[37] for U^{VI}–O bond and the data of Brese and O'Keeffe[38,39] for K−O,K−Br, K−F, Rb−O,Cs−Oand Ge−Obonds. The BVS results are given in Supporting Information **Table S2**.

3. RESULTS AND DISCUSSION

3.1 Crystal Growth

Two conventional techniques (Hydrothermal and HT flux growth) and High-temperature/High-pressure method (HT/HP) were applied for the synthesis of uranyl germanates in this work. NH_4Cl as a mineralizer helps the formation of larger, higher quality crystals, which has been applied for the syntheses ofzeolite[40] and other oxides[41,42]. Hydrothermal experiments were performed for the synthesis of$\boldsymbol{A}^+(UO_2)(HGeO_4){\cdot}H_2O$ ($\boldsymbol{A}^+$ = Rb^+, Cs^+) using NH_4Cl as a mineralizer.[43]We found that this mineralizer is necessary for the synthesis of $Rb_6(UO_2)_3(Ge_2O_7)_2{\cdot}0.5H_2O$crystals. In order to improve the yield of the crystal, we systematically explore different experiment conditions (reaction time and cooling rate) and molar ratios of reagents. However, all these changes did not increase the yield and crystal quality.

Additionally, we attempted synthesis of the isomorphous/isotypical cesium phase and used CsOH to replace RbOH under the same synthetic condition, but the experiments were unsuccessful.

In the high temperature flux experiments, two distinct compounds including $K_8BrF(UO_2)_3(Ge_2O_7)_2$, and $Cs_6(UO_2)_2Ge_8O_{21}$ were obtained using different mixed fluxes (KF–KBr, and CsF–CsCl, respectively). Alkali halides can dissolve the initial chemicals especially for oxides (SiO_2/GeO_2, UO_3/U_3O_8), and they have a low volatility and can be easily removed from the reaction products with water.[27,44] Compared to the influence of single flux, mixed fluxes can extremely reduce the melting temperature of the reagents.[45] It is worth to note that salt-inclusion units can be generated within the crystal growth process using mixed halide fluxes. These salt inclusion fragments filled the large pores of anionic frameworks.

The high-pressure conditions facilitate the special reactions in the high-temperature melts compared to the traditional method. The influence of extreme condition for the synthesis of actinide oxo-anions has been explored, and the method resulted in the formation of some unusual compounds with mixed-valence or mixed-coordination geometries such as $Th(As^{III}_4As^{V}_4O_{18})$[31] and $Th_2Te_3O_{11}$.[34] The previous works demonstrate that high-pressure condition shifts the oxygen based coordination environment of central Ge-atoms from 4 to 6.

3.2 Crystal Structure

$K_8BrF(UO_2)_3(Ge_2O_7)_2$. The structure of $K_8BrF(UO_2)_3(Ge_2O_7)_2$ crystallizes in triclinic ***P***-1 space group, and it consists of two primary building units (PBUs) including uranyl tetragonal bipyramids and germanate tetrahedra (**Figure 1**).The isolated $(UO_6)^{6-}$ tetragonal bipyramids have two short U=O bonds with an average bond length of 1.821 Å and four long U–O bonds within

an average 2.235 Å.[46] Germanate tetrahedra exhibit the average Ge–O bond distances of 1.726 Å. $[Ge_2O_7]^{6-}$ units are formed via vertex sharing of two Ge tetrahedra, and Ge–O–Ge angle is 126(1)°. The linkage of these PBU's leads to the formation of anionic uranyl germanate framework with 12-membered channels of 8.20 × 4.89 $Å^2$(measured from the centers of the nearest oxygen atoms). The BVS for U(1), U(2), U(3), Ge(1) and Ge(2) sites are 5.65, 6.04, 5.80, 4.28 and 4.26 v.u., respectively, which are in a good agreement with the expected oxidation states of $U^{VI}$and Ge^{IV}.

Potassium cations, disordered Br^- and F^- anions in the structure of $K_8BrF(UO_2)_3(Ge_2O_7)_2$ are located in the center of 12-membered channels. The coordination environments of K-cations are 8 for K1, 10 for K2, 8 for K3, and 7 for K4. The Br^- anions are coordinated on six K cations, forming $[K_6Br]^{5+}$ distorted trigonal prism. The F^- anions coordinate five K cations, forming $[K_5F]^{4+}$ distorted square pyramidal geometry, as plotted in **Figure 1d**. K–Br bond lengths range from 3.075(8) to3.465(7) Å in the $[K_6Br]^{5+}$ distorted trigonal prism.The average value of K–Br bond lengths for the $[K_6Br]^{5+}$ units (~ 3.261 Å) is smaller than that for alkali metal halide KBr (3.299 Å). The result of BVS calculation of Br^- anions is 1.04 v.u., which is correspondent with the expected value. The similar salt-inclusion unit has been reported in the uranyl silicate with $[Cs_6F]^{5+}$ units.[5] In the $[K_5F]^{4+}$ distorted square pyramidal geometry, the K–F bond lengths range from 2.56(3) to3.39(3) Å.BVS analysis for F^- ions yields 0.63 v.u., demonstrating F^- ions bond weakly K cations by forming longer K–F bonds.

The anionic framework of $K_8BrF(UO_2)_3(Ge_2O_7)_2$provides large voids for the existence of $[K_8BrF]^{6+}$ chains. Moreover, isolated uranyl cations (charge is +2) link $[Ge_2O_7]^{6-}$ units (charge is -3 per Ge cation) generating the anionic framework with the relatively low negative charge of -6,

which is compensated by $[K_8BrF]^{6+}$ inclusion units. We used the Calc Solv program in Platon package[47] for calculation of the volume of 12-membered channels in the structure of $K_8BrF(UO_2)_3(Ge_2O_7)_2$. It has been found to be 252.8 $Å^3$/unit cell after deleting the $[K_8BrF]^{6+}$ salt-inclusion unit.

Topology of $K_8BrF(UO_2)_3(Ge_2O_7)_2$ along ***a*** axis is plotted in **Figure 2.** We cut the channel into an unfolding wall, as shown in **Figure 2b**, in order to recognize the U-Ge interconnections of the 12-membered channel. It can be seen that the channel is assembled from two different types of SBUs - $[UGe_4]$ pentamers of **A-** and **A2-** types.$[UGe_4]$ pentamers of **A-**type form a typical one-dimensional chain via connecting the sameSBUs. The similar infinite chain has been found in the structure of $K_2Ca_4(UO_2)(Si_2O_7)_2$.[48]$[UGe_4]$ pentamers of **A2-**type are the linkers resulting in the formation of unfolding wall with a SBU stacking sequence of **A-A2-A-A-A2-A**. The wall displays the presence of 6- and 8-membered ring windows. The nearly ideal hexagonal prism in the structure of $K_8BrF(UO_2)_3(Ge_2O_7)_2$, as shown in **Figure 2c,** was obtained by gluing the wall constructed from SBUs. Blue and dark red rectangles represent SBUs $[UGe_4]$ pentamers (**A** type) and (**A2** type), respectively. Another type of 12-membered channel in the salt-inclusion uranyl germanate compounds such as $[KK_6Cl][(UO_2)_3(Ge_2O_7)_2]$, $NaK_6Cl(UO_2)_3(Ge_2O_7)_2$and $[Cs_6Ag_2Cl_2][(UO_2)_3(Ge_2O_7)_2]$was found,[2,3]but it is composed of **A** type and **A1** types. The difference between both structures is based on the cationic arrangement within 12-membered channels. The ideal 3D skeleton of the whole structure of $K_8BrF(UO_2)_3(Ge_2O_7)_2$ is built upon the concept of SBUs in **Figure 3**. We can see that the above discussed 1D blue chains consisting of $[UGe_4]$ pentamers (**A** type) and joined the dark red rectangles ($[UGe_4]$ pentamers (**A2** type)) via corner sharing, resulting in the formation of the ideal 3D model.

$Rb_6(UO_2)_3(Ge_2O_7)_2{\cdot}0.5H_2O$. The three dimensional structure of $Rb_6(UO_2)_3(Ge_2O_7)_2{\cdot}0.5H_2O$ was refined in triclinic syngony within centrosymmetric ***P***-1 space group. The asymmetric units in the structure contain three U, two Ge and four Rb sites. U cations coordinated six O atoms form independent uranyl tetragonal bipyramids with average U=O bonds of 1.799 Å and the linear O=U=O uranyl group. The U–O bonds in the equatorial plane of each tetragonal bipyramids display longer distances (average 2.233 Å). Each Ge cation bridged four O atoms to produce germanate tetrahedra with the average Ge–O bonddistances of 1.729 Å. O–Ge–O angles in the germanate tetrahedra vary from 100.6(5)° to 116.0(7)°. Pyro-germanate $[Ge_2O_7]^{6-}$ groups form via sharing common O atom of two tetrahedra, and Ge–O–Ge angle is ~128.9(7)°. The $[Ge_2O_7]^{6-}$ groups link the isolated uranyl tetragonal bipyramids by sharing corners, producing a novel 3D uranyl germanate framework with hexagon shaped 12-membered channel, as plotted in **Figure 4**. The channel size is ~ 8.36 × 5.03 $Å^2$, which is larger than the dimension of the channel in the structure of the above-discussed $K_8BrF(UO_2)_3(Ge_2O_7)_2$. Rb cations in the structure of $Rb_6(UO_2)_3(Ge_2O_7)_2{\cdot}0.5H_2O$ are within the channels, compensating the negative charge of the anionic framework. Additionally, H_2O molecules are located at the center of the channels, occupying the rest of the space within the framework. The framework contains two types of SBUs $[UGe_4]$ pentamers of **A-** and **A2-**type, whichis the same with the structure of$K_8BrF(UO_2)_3(Ge_2O_7)_2$ obtained by HT flux growth method.

The previously reported uranyl germanate compound $Cs_6(UO_2)_3(Ge_2O_7)_2{\cdot}4H_2O$[22]with 12-membered channels has similar chemical composition with $Rb_6(UO_2)_3(Ge_2O_7)_2{\cdot}0.5H_2O$, and difference is only in alkali metal cations and the quantity of H_2O molecules located at the center of the channels. However, the structure of $Cs_6(UO_2)_3(Ge_2O_7)_2{\cdot}4H_2O$ is composed of **A** and **A1** types of SBUs $[UGe_4]$ pentamers, as plotted in **Figure S3.** Additionally,

$K_4Na_2(UO_2)_3(Ge_2O_7)_2{\cdot}3H_2O$[49] and $Na_3K_3[(UO_2)_3(Si_2O_7)_2]{\cdot}2H_2O$[50] from $\boldsymbol{A}_6(UO_2)_3(\boldsymbol{T}_2O_7)_2{\cdot}xH_2O$ (***T*** = Si, Ge) family, consist of **A** and **A2** types of $[UGe_4]$ pentamers, which is similar to the structure of $Rb_6(UO_2)_3(Ge_2O_7)_2{\cdot}0.5H_2O$. However, $K_4Na_2(UO_2)_3(Ge_2O_7)_2{\cdot}3H_2O$ has 14-membered channels, and $Na_3K_3[(UO_2)_3(Si_2O_7)_2]{\cdot}2H_2O$ has a 2D layer structure containing 8-membered rings.

$Cs_6(UO_2)_2Ge_8O_{21}$. $Cs_6(UO_2)_2Ge_8O_{21}$ crystallizes in the centrosymmetric ***P***-1 space group (**Figure 5**). The structure consists of two uranyl sites, four cesium sites, four germanium sites and 13 oxygen atoms. Both uranyl cations bonding six oxygen atoms creating uranyl tetragonal bipyramids with the typical U=O bond lengths (1.824(5) Å for U(1) and U(2)) and linear O=U=O bonds. The longer equatorial U–O bonds are in the range of 2.217(5) – 2.263(5) Å. Ge(2) forms adistorted tetrahedron with the Ge–O bonds ranging from 1.720(5) to 1.760(5) Å. The remaining Ge cations form trigonal bipyramids coordinating five O atoms. The lengths of Ge–O bonds are from 1.692(6) Å to 2.202(8) Å, and the O–Ge–O angles vary between 67.6(3)° and 169.7(3)°. These three germanium trigonal bipyramids are bonded together by edge sharing to form Ge_3O_{11} clusters, which share corners with Ge(2) tetrahedra to form a novel open-branched dreier single germanate layer (according to Liebau notation[51]), as it is shown in **Figure 5b**. The layers are projected along [110] plane and based upon 3- and 8-membered germanate rings. The Ge–O–Ge bond angles in the layer vary between 91.3(3)° and 138.9(5)°. The similar layer was observed recently by Morrisonet al[52] in a rare earth silicate compound where the $[Si_4O_{10}]$ silicate layers constructed by the corner sharing of SiO_4 tetrahedra. To the best of our knowledge, the germanate layer containing 4- and 5-coordinated Ge has never been reported before. The germanate layers are bridged by UO_6 polyhedra producing 3D framework with 10-membered rings. Cs cations fitting into the voids of the framework show diverse coordination geometry: 8

for Cs(1), 11 for Cs(2), 9 for Cs(3), 7 for Cs(4).BVS analysis for U, Ge and Cs cations are in a good agreement with the expected 6+, 4+ and 1+ oxidation states, respectively. BVS result for O(1) yield 1.25 v.u., which is attributed to that the O(1) only bonds one Cs cation and three Ge cations by longer Ge–O bond lengths of 2.011(8) – 2.202(8) Å.

The projection of $Cs_6(UO_2)_2Ge_8O_{21}$structure along ***a*** axis is plotted in **Figure 6.** It is easy to see that polymerization of two SBUs results in the formation of the three-dimensional structure. The first SBU is $[UGe_4]$ pentamers (**$4^2.5^2$-A2** type) composed of two Ge tetrahedra and two Ge trigonal bipyramids with one uranyl tetragonal bipyramid (**Figure 6a**). One 4-coordinated Ge in the SBUs bonds 5-coordinated Ge to create $[Ge_2O_8]$ groups. Second SBU is $[UGe_4]$ pentamers (**5^4-A2** type) formed by four Ge trigonal bipyramids connected to one UO_6 polyhedron in **Figure 6c**. The rich coordination environment of Ge cations expands the variety of SBUs, which further leads to the complexity of the uranyl germanate structures.

$A^+_2(UO_2)_3(GeO_4)_2$ (A^+ = Rb$^+$, Cs$^+$). The structures of these two similar compounds have been solved in orthorhombic system within centrosymmetric ***P***nma space group. The calculated densities for the Rb and Cs oxo-compounds are 6.547 and 6.831 g/cm^{-3}, which are larger than for other above-discussed compounds. The framework projection of $Cs_2(UO_2)_3(GeO_4)_2$ along ***b*** axis shown in **Figure 7a** and consists of three U, one Ge, one Cs and 11 O crystallographically independent atoms. Uranium cations are bonded by two O atoms at short distances ranging from 1.793(6) to 1.813(6) Å, creating nearly linear uranyl $(UO_2)^{2+}$ ions. The longer U–O equatorial bond lengths vary between 2.284(3) and 2.567(5) Å. The UO_7 bipyramids through sharing edges produce typical $[UO_5]_\infty$uranyl chains extending along ***b*** axis, as plotted in **Figure 7b**. BVS analysis yields 5.84, 5.88 and 5.85 v.u. for U(1), U(2) and U(3) cations, respectively. Ge cations

are presented only in GeO_5 trigonal bipyramids via linking five O atoms, and the Ge–O bond lengths are from 1.760(4) to 2.041(1) Å. Each trigonal bipyramid shares two of its vertices with two adjacent bipyramids to create infinite $[GeO_5]_\infty$ chains extending along ***b*** axis. Two types of chains, $[UO_5]_\infty$uranyl and $[GeO_5]_\infty$trigonal bipyramids chains, are connected through edge-sharing into the 3D framework with oval-shaped 12-membered channels along ***b*** axis. The framework is similar to the structure of $Ag_2(UO_2)_3(GeO_4)_2{\cdot}2H_2O$[20] synthesized under hydrothermal condition. The dimensions of the channels are ~ 3.910 × 8.516 $Å^2$. Cs cations reside in the center of the channels and possess 10-coordinated environment. BVS analysis yields 3.98, and 1.32 v.u. for Ge(1), and Cs(1) cations, respectively. The structure of $Rb_2(UO_2)_3(GeO_4)_2$ has smaller size of channels ~ 3.670 × 8.578 $Å^2$. Additionally, Ge–O–Ge and U–O–U bond angles in $Cs_2(UO_2)_3(GeO_4)_2$ are larger compared to that in $Rb_2(UO_2)_3(GeO_4)_2$. Gagné et al. have found that the maximum Rb–O and Cs–O bond lengths in 10-coordinated environment are 3.890 and 3.986 Å, respectively.[53] For the compound $Cs_2(UO_2)_3(GeO_4)_2$, the maximum Cs–O bond length in 10-coordinated environment is 3.713 Å (< 3.986 Å). However, for $Rb_2(UO_2)_3(GeO_4)_2$ the maximum Rb–O bond length in 10-coordinated environment is 3.936 Å (> 3.890 Å). Therefore, Rb cations can be assigned to have the 9-coordinated geometries, and Rb–O bond lengths are in the range of 2.786(4) ~ 3.565(4) Å (< 3.839 Å, the maximum value of Rb–O bond length in 9-coordinated environment).

The interconnection types of 12-membered channels have been analyzed by using the method of SBUs and the cutting and gluing strategies. The channel has been unfolded from a germanate chain into a sheet, and the corresponding representation is shown in **Figure 7d.** The idealized and unfolded sheet can be constructed by the SBU $[U_2Ge_2]$ tetramers (**E** type) (**Figure 7c**). The

SBU consists of two UO_7 pentagonal bipyramids and two GeO_5 trigonal bipyramids. The entire structure is built upon the assembly of 12-membered channels by sharing SBU [U_2Ge_2] tetramers. Comparing to the known phases, the two dimensional structures of $LiUNbO_6$[54] and $Li_4[(UO_2)_2(W_2O_{10})]$[55] are similar to the unfolding sheet of $Cs_2(UO_2)_3(GeO_4)_2$. However, the structure of $LiUNbO_6$ was composed of UO_7 pentagonal bipyramids and NbO_5 square pyramids. The structure of $Li_4[(UO_2)_2(W_2O_{10})]$ consisted of UO_7 pentagonal bipyramids and WO_6 octahedra.

3.3 Structural features of uranyl germanates

The synthetic methods, U/Ge ratios, U=O and U−O bond lengthsof all reported uranyl germanates have been summarized, and their structures have been classified by the uranyl/germanate dimensionality and SBUs, as presented in **Table 2**. Four different methods includinghydrothermal, HT, HT/HP and HT/HP hydrothermal methods have been used for the synthesis of uranyl germanates, and most of phases were synthesized by the hydrothermal and HT methods. HT/HP hydrothermal method was used for the synthesis of mixed-valence uranium germanates,[25,26] and only one pure U(VI) germanate, $Cs_6((UO_2)_3(Ge_2O_7)_2)(H_2O)_4$,[22] was obtained up to now.

The structures of these phases contain different uranyl units, which includes the 0-D isolated uranyl tetragonal bipyramid, 1-D uranyl pentagonal and tetragonal chains (only for $Cs_2(UO_2)GeO_4$[2] and 2-D uranyl pentagonal layers (only for ($Mg[(UO_2)_2(Ge_2O_6(OH)_2)](H_2O)_{4.4}$)[56].Additionally, HT synthetic condition only resulted in the formation of 0-D isolated uranyl tetragonal bipyramid except for $Cs_2(UO_2)GeO_4$. 1-D uranyl pentagonal bipyramid chains can be observed in the phases formingin the hydrothermal and HT/HP conditions. The structures of uranyl germanates contain 0-D germanate units, 1-D

germanate trigonal bipyramidal chain and 2-D germanate layers. Among them, 0-D germanate units include single GeO_4 tetraheda, Ge_2O_7 and Ge_2O_8 pyro-germanate groups,Ge_4O_{12}square-unites,and Ge_8O_{22} poly-germanate clusters. The germanate units do not show any obvious relation with the synthetic methods of uranyl germanates.

The U/Ge ratio in the uranyl germanatesis related to the dimensionality of uranyl/germanate units and types of SBUs. The uranyl germanates with U/Ge ratios below 0.75 posses0-D isolated uranyl tetragonal bipyramid except for $(Cu(H_2O)_4)((UO_2)(HGeO_4))_2(H_2O)_2$[57], and only the compounds with U/Ge ratio of 1.5 contain 1-D germanate trigonal bipyramids. Most of the structures with U/Ge ratios of below 0.75 represent the **A** type of SBUs.

The SBUs extracted from all reported uranyl germanate compounds without uranyl cation-cation interactions are presented in **Figure 8**. The structures of uranyl germanates contain various SBUs, and several compounds are composed of two or three **A**-type SBUs. Except for $Cs_2(UO_2)GeO_4$, H-T synthetic condition only leads to the formation of **A**-type SBUs, which is related to the existence of 0-D isolated uranyl tetragonal bipyramid in the structures. **D**- and **E**-type SBUs can be observed in the structures of compounds synthesized by hydrothermal and H-T/H-P conditions.It can be seen in **Table 2** that the U=O and U–O bond lengths of uranyl phases depend on the coordination number of uranyl cations, which have been mentioned by Burns et al.[37] U=O bond lengths in the1-D uranyl pentagonal bipyramid chains (< 1.81Å for most of structures) are shorter than that in the 0-D isolated uranyl tetragonal bipyramids (>1.82Å for most of structures).The average U–O bond lengthsin uranyl pentagonal bipyramids are longer than that in uranyl tetragonal bipyramids, further indicating the influence of synthetic methods to the U=O and U–O bond lengths.

3.4. Raman and Infrared Spectral Analysis

The three compounds, $K_8BrF(UO_2)_3(Ge_2O_7)_2$, $Rb_6(UO_2)_3(Ge_2O_7)_2{\cdot}0.5H_2O$, and $Cs_6(UO_2)_2Ge_8O_{21}$, present centrosymmetric structures with C_i point group and contain one formula unit per unit cell.In the structure of $K_8BrF(UO_2)_3(Ge_2O_7)_2$, U atoms are located at 1e, 1f, and 1a sites, and the remaining atoms occupy 2i sites. Mechanical representation of the vibrations of the structure investigated by group theoretical approach[58] is $54A_g + 63A_u$, as shown in **Table 3**. The acoustic modes are the same as $Rb_6(UO_2)_3(Ge_2O_7)_2{\cdot}0.5H_2O$. The vibrationsof $K_8BrF(UO_2)_3(Ge_2O_7)_2$ contains $60A_u$IR-active modes and $54A_g$ Raman-active modes. **Figure 9**shows Raman spectrum of $K_8BrF(UO_2)_3(Ge_2O_7)_2$ in the 100 − 1000 cm^{-1} region. The $\nu_1(UO_2)^{2+}$ modes appear at 705 and 739 cm^{-1}, and the $\nu_3(UO_2)^{2+}$ modes are found and located at 803, 841 and 869 cm^{-1}. Six $\nu_2(UO_2)^{2+}$ bending modes can be seen in the 200 − 330 cm^{-1} range. The ν_3 antisymmetric vibrational modes of $(GeO_4)^{4-}$ units contribute to the band at 639 cm^{-1}.[59] The ν_1(Ge−O−Ge) vibrations of Ge_2O_7 units appear at 551 and 512 cm^{-1}. In the literature, Raman spectra of pyro-germanates containing inorganic phases exhibit similar bands.[26, 60,61] The weak band at 401 cm^{-1} is assigned to the ν_2(O−Ge−O) vibrations.[59] Three bands at 131, 143 and 158 cm^{-1} may correspond to the combinations of two vibrational modes including K^+ cations and Ge_2O_7 groups.[62] In the low frequency 100 − 400 cm^{-1}regions some peaks may correspond to the bending modes of salt-inclusion units.[63,64]

Uranium cations in $Rb_6(UO_2)_3(Ge_2O_7)_2{\cdot}0.5H_2O$ occupy three nonequivalent sites of 1d, 1h, and 1c. H_2O molecules are at 1b sites. The remaining Rb cations, Ge cations, and O ions are at 2i sites. Infrared and Raman actives in the centrosymmetric structure only show the A_u and A_g modes, respectively. The resulting 108 zone-center vibrational modes are distributed the following mechanical representation of C_i :$\Gamma_{vib} = 48A_g + 60A_u$, where $3A_u$ corresponds toacoustic modes, $57A_u$ corresponds to the IR active modes and $48A_g$ represents the Raman

modes (**Table 3**). The Raman spectrum of $Rb_6(UO_2)_3(Ge_2O_7)_2{\cdot}0.5H_2O$ is given in **Figure 9**. Four bands at 707, 721, 743 and 783 cm^{-1} can be assigned to the $\nu_1(UO_2)^{2+}$ modes, and the band at 837 cm^{-1} is attributed to the $\nu_3(UO_2)^{2+}$vibrations. The bands of ν_1(Ge−O−Ge) and ν_2(O−Ge−O) modes can be found at 545 and 400 cm^{-1}, respectively. The high intense band at 107 cm^{-1} may be due to the phonon modes and the translations of Rb cations. Three bands at 2869, 2928 and 2969 cm^{-1} appear in the high frequency region of the Raman spectrum of $Rb_6(UO_2)_3(Ge_2O_7)_2{\cdot}0.5H_2O$, and these bands are due to the possible $\nu_3(H_2O)$ vibrations.[61,65]

Both U atoms in the structure of $Cs_6(UO_2)_2Ge_8O_{21}$ occupy the 1c and 1b sites, respectively. The rest atoms are at 2i sites. The mechanical representation is as follows: $\Gamma_{vib} = 63A_g + 69A_u$,which have $66A_u$ IR-active modes and $63A_g$ Raman active modes. Experimental Raman spectrum of single crystal $Cs_6(UO_2)_2Ge_8O_{21}$ presents the strong symmetric stretching vibrations ($\nu_1(UO_2)^{2+}$) of uranyl ions, which are located at 711, 734 and 751 cm^{-1}. Several weak bands between 800 and 950 cm^{-1} is attributed to the $\nu_3(UO_2)^{2+}$ modes.[65,66] The $\nu_2(UO_2)^{2+}$bending vibrations are found to lie at 220, 240, 264, 305 and 354 cm^{-1}.[67] Interestingly, the region of middle frequency displays lots of peaks, which are related to the germanate layer in the crystal structure. The band at 678 cm^{-1} is assigned to the $\nu_3(GeO_4)^{4-}$antisymmetric vibrations.[59]Two sharp and intense peaks at 548, 596 cm^{-1} and a shoulder at 578 cm^{-1}can be assigned to ν_1(Ge–O–Ge) vibrations.[62,68,69] The ν_1(Ge–O–Ge) vibrations in germanate rings appear at 503 cm^{-1}.[62,68] The ν_4(O–Ge–O) bending vibrations are located at 427, 446 and 477 cm^{-1}.[62] The Raman spectra in the low frequency region between 100 and 200 cm^{-1} presents five bands. The bands at 117, 132 and 195 cm^{-1} may be attributed to the translations of Cs cations and germanate rings.[62] The remaining two bands at 153 and 166 cm^{-1} may be assigned to the librations of the germanate rings.[68]

Two compounds, $\boldsymbol{A}^{+}_2(UO_2)_3(GeO_4)_2$ ($\boldsymbol{A}^{+}$ = Rb^{+}, Cs^{+}), are iso-structural and their vibrational modes are characterized by the following mechanical representation: $\Gamma_{vib} = 37A_g + 26A_u + 26B_{1g} + 37B_{1u} + 37B_{2g} + 26B_{2u} + 26B_{3g} + 37B_{3u}$. 97 of the vibrations correspond to the IR-active modes ($\Gamma_{IR} = 36B_{1u} + 25B_{2u} + 36B_{3u}$,) and 126 of the vibrations correspond to Raman active modes ($\Gamma_{Raman} = 37A_g + 26B_{1g} + 37B_{2g} + 26B_{3g}$). Raman spectra of $\boldsymbol{A}^{+}_2(UO_2)_3(GeO_4)_2$ ($\boldsymbol{A}^{+}$ = Rb^{+}, Cs^{+}) are given in **Figure 9**. By comparison, we can see that most of bands in the Raman spectrum of $Cs_2(UO_2)_3(GeO_4)_2$ shift to high frequency for $Rb_2(UO_2)_3(GeO_4)_2$. Additionally, the empirical expressions of Bartlett and Cooney[70] are used to obtain the theoretical values of $\nu_1(UO_2)^{2+}$ and $\nu_3(UO_2)^{2+}$ vibrations. By calculation, the U=O bond lengths in the uranyl $(UO_2)^{2+}$ ionsprovide the average bands at 809(ν_1) / 878(ν_3) cm^{-1} for $Cs_2(UO_2)_3(GeO_4)_2$ and 807(ν_1) / 874(ν_3) cm^{-1} for $Rb_2(UO_2)_3(GeO_4)_2$, respectively. The measured Raman spectra of both compounds exhibited some intense bands (813(ν_1) / 870(ν_3) cm^{-1} for $Cs_2(UO_2)_3(GeO_4)_2$ and 818(ν_1) / 867(ν_3) cm^{-1} for $Rb_2(UO_2)_3(GeO_4)_2$), which are in good agreement with the calculated results.

Some sharp peaks at 721, 753 and 781 cm^{-1} appear in the spectra of $Cs_2(UO_2)_3(GeO_4)_2$, and they are attributed to the $\nu_1(UO_2)^{2+}$ vibrations. Five bands at 830, 836, 851, 870 and 909 cm^{-1} are associated with the $\nu_3(UO_2)^{2+}$ vibrations. Similar results can be found in the Raman spectra of the uranyl tellurium compounds[71] synthesized by HT/HP technique. The bands in the 200 – 340 cm^{-1} region are assigned to the $\nu_2(UO_2)^{2+}$ vibrations. Two broad and intense bands at 404 and 422 cm^{-1} is attributed to the ν_4(O–Ge–O) vibrations.[62] The bands in the 100 – 200 cm^{-1}region may be attributed to the mixing vibrations of Cs translations and ν_2(O−Ge−O) modes.[59] Compared to $Cs_2(UO_2)_3(GeO_4)_2$, a weak band at 512 cm^{-1} was found in the Raman spectra of $Rb_2(UO_2)_3(GeO_4)_2$, which corresponds to the ν_1(Ge–O–Ge) vibrations.

To-date, most of synthetic U−Ge−O phases reported previously has been characterized by Infrared spectroscopy. **Figure S4** shows the Infrared spectrum of $Cs_6(UO_2)_2Ge_8O_{21}$in the 400 − 1000 cm^{-1} region. Three bands at 857, 878 and 945 cm^{-1} correspond to the $\nu_3(UO_2)^{2+}$ modes.[20,22] Two bands at 797, 808 may be attributed to the mixing vibrations of $\nu_3(GeO_4)$ and $\nu_3(UO_2)^{2+}$ modes.[20,72] A strong peak at 755 cm^{-1} and three shoulders at 678, 693 and 735 cm^{-1} are caused by the ν_3(Ge–O–Ge) vibrations.[20] Four weak bands at 520, 545, 582 and 591 cm^{-1} are due to the ν_1(Ge–O–Ge) vibrations.[62] Two weak bands at 445 and 483 cm^{-1} may be caused by the $\nu_4 + \nu_2$ mixing bending vibrations of O−Ge−O bonds.[62,72] The low frequency band at 407 cm^{-1} is due to the Cs translations and the rocking of O−Ge−O bonds.[30]

4. Conclusions

Conventionaland extreme synthetic conditions including hydrothermal and HT flux growth and HT/HP technique have been used for the synthesis of five new compounds in uranyl germanate family. Their structures have been characterized by X-ray crystallographic analysis and Raman/IR spectroscopy. By comparison with the previously reported uranyl compounds, we found a significant level of similarity between $\boldsymbol{A}_6(UO_2)_3(\boldsymbol{T}_2O_7)_2{\cdot}xH_2O$ ($\boldsymbol{T}$ = Si, Ge) or $K_8BrF(UO_2)_3(Ge_2O_7)_2$ and $Rb_6(UO_2)_3(Ge_2O_7)_2{\cdot}0.5H_2O$ obtained by different methods. The anionic framework with $[(UO_2)_3(\boldsymbol{T}_2O_7)_2]^{6-}$ composition exhibits several different structural motifs with 2D layer and 3D frameworks. The 3D frameworks also have internal differentiation and can be based upon 8-, 12- or 14-membered channels. Importantly, the presence of rare $[K_8BrF]^{6+}$ fragments consisting of distorted $[K_6Br]^{5+}$ trigonal prism and $[K_5F]^{4+}$ square pyramids in $K_8BrF(UO_2)_3(Ge_2O_7)_2$ indicates a wide range of stability of salt-inclusion units in uranium based family. The coordination geometries of uranium and germanium cations are affected by the

synthetic conditions, which result in the formation of novel SBUs. Group theory analysis, Raman and infrared spectra show the vibrational modes for these unique centrosymmetric triclinic and orthorhombic crystal structures.

Conflicts of interest

There are no conflicts to declare.

Acknowledgments

This research was supported by the DFG under grant AL1527/3-1. We thank Dr. Martina Klinkenberg (IEK-6, Forschungszentrum Jülich) for SEM/EDX measurements, and Dr. Hartmut Schlenz for collection of Raman spectra, and Mrs. Norman Lieck for collection of Infrared spectra. Dr. H.J. Li thanks the Chinese Scholarship Council for financial support.

References

1 C. S. Lee, S. L. Wang, Y. H. Chen and K. H. Lii, *Inorg. Chem.*, 2009, **48(17)**, 8357-8361.

2 H. J. Li, E. M. Langer, P. Kegler, G. Modolo and E. V. Alekseev, *Inorg. Chem.*, 2018, **57(17)**, 11201-11216.

3 C. A. Juillerat, E. E. Moore, G. Morrison, M. D. Smith, T. Besmann and H. C. Zur Loye, *Inorg. Chem.*, 2018, **57(18)**, 11606-11615.

4 G. Morrison, T. T. Tran, P. S. Halasyamani and H. C. zur Loye, *Inorg. Chem.*, 2016, **55(7)**, 3215-3217.

5 G. Morrison, M. D. Smith and H. C. Zur Loye, *J. Am. Chem. Soc.*, 2016, **138(22)**, 7121-7129.

6 X. Bu, P. Feng and G. D. Stucky, *Chem. Mater.* , 2000, **12(6)**, 1505-1507.

7 L. D. Sanjeewa, M. A. McGuire, C. D. McMillen, O. O. Garlea and J. W. Kolis, *Chem. Mater.* , 2017, **29(3)**, 1404-1412.

8 N. R. Spagnuolo, G. Morrison and H.-C. z. Loye, *Solid State Sci.*, 2019, **97**, 105973.

9 H. J. Li, P. Kegler, V. V. Klepov, M. Klinkenberg, D. Bosbach and E. V. Alekseev, *Inorg. Chem.*, 2018, **57(11)**, 6734-6745.

10 G. Morrison, M. D. Smith, T. T. Tran, P. S. Halasyamani and H.-C. z. Loye, *Cryst. Eng. Comm.*, 2015, **17**, 4218-4222.

11 G. Morrison, M. D. Smith and H. C. Zur Loye, *Inorg Chem*, 2017, **56(3)**, 1053-1056.

12 X. Wang, J. Huang, L. Liu and A. J. Jacobson, *J. Mater. Chem.*, 2002, **12**, 406-410.

13 H.-K. Liu, W.-J. Chang and K.-H. Lii, *Inorg. Chem.* , 2011, **50**, 11773-11776.

14 C.-S. Chen, H.-M. Kao and K.-H. Lii, *Inorg. Chem.* , 2005, **44**, 935-940.

15 J. Huang, X. Wang and A. J. Jacobson, *J. Mater. Chem.*, 2003, **13**, 191-196.

16 J. Plasil, K. Fejfarova, J. Cejka, M. Dusek, R. Skoda and J. Sejkora, *Am. Mineral.*, 2013, **98**, 718-723.

17 D. Waroquiers, X. Gonze, G.-M. Rignanese, C. Welker-Nieuwoudt, F. Rosowski, M. Göbel, S. Schenk, P. Degelmann, R. André, R. Glaum and G. Hautier, *Chem. Mater.*, 2017, **29(19)**, 8346-8360.

18 C. M. Wang, C. W. Yang, C. H. Lin and K. H. Lii, *Inorg. Chem.*, 2010, **49(22)**, 10229-10231.

19 T. Conradsson, X. Zou and M. S. Dadachov, *Inorg. Chem.*, 2000, **39(8)**, 1716-1720.

20 J. Ling, J. M. Morrison, M. Ward, K. Poinsatte-Jones and P. C. Burns, *Inorg. Chem.*, 2010, **49(15)**, 7123-7128.

21 J. M. Morrison, L. J. Moore-Shay and P. C. Burns, *Inorg. Chem.*, 2011, **50(6)**, 2272-2277.

22 C. H. Lin, R. K. Chiang and K. H. Lii, *J. Am. Chem. Soc.*, 2009, **131(6)**, 2068-2069.

23 Q. B. Nguyen, C. L. Chen, Y. W. Chiang and K. H. Lii, *Inorg. Chem.*, 2012, **51(6)**, 3879-3882.

24 Q. B. Nguyen and K. H. Lii, *Inorg. Chem.*, 2011, **50(20)**, 9936-9938.

25 Q. B. Nguyen, H. K. Liu, W. J. Chang and K. H. Lii, *Inorg. Chem.*, 2011, **50(10)**, 4241-4243.

26 C. H. Lin and K. H. Lii, *Angew. Chem. Int. Ed. Engl.*, 2008, **47(45)**, 8711-8713.

27 D. E. Bugaris and H. C. zur Loye, *Angew. Chem. Int. Ed. Engl.*, 2012, **51(16)**, 3780-3811.

28 C. D. McMillen and J. W. Kolis, *Dalton Trans.* , 2016, **45**, 2772-2784.

29 S. Wu, S. Wang, M. Polinski, O. Beermann, P. Kegler, T. Malcherek, A. Holzheid, W. Depmeier, D. Bosbach, T. E. Albrecht-Schmitt and E. V. Alekseev, *Inorg. Chem.*, 2013, **52(9)**, 5110-5118.

30 S. Wu, O. Beermann, S. Wang, A. Holzheid, W. Depmeier, T. Malcherek, G. Modolo, E. V. Alekseev and T. E. Albrecht-Schmitt, *Chem. – Eur. J.*, 2012, **18(14)**, 4166-4169.

31 N. Yu, V. V. Klepov, P. Kegler, D. Bosbach, T. E. Albrecht-Schmitt and E. V. Alekseev, *Inorg. Chem.*, 2014, **53(16)**, 8194-8196.

32 N. Yu, P. Kegler, V. V. Klepov, J. Dellen, H. Schlenz, E. M. Langer, D. Bosbach and E. V. Alekseev, *Dalton T.*, 2015, **44(47)**, 20735-20744.

33 B. Xiao, P. Kegler, D. Bosbach and E. V. Alekseev, *Inorg. Chem.*, 2016, **55(9)**, 4626-4635.

34 B. Xiao, P. Kegler, D. Bosbach and E. V. Alekseev, *Inorg. Chem.*, 2017, **56** 2926-2935.

35 G. M. Sheldrick, *Acta Crystallogr. A*, 2008, **64**, 112-122.

36 A. L. Spek, *Acta Crystallogr. D* 2009, **65**, 148-155.

37 P. C. Burns, R. C. Ewing and F. C. Hawthorne, *Can. Mineral.*, 1997, **35**, 1551-1570.

38 N. E. Brese and M. Okeeffe, *Acta Crystallogr B*, 1991, **47**, 192-197.

39 I. D. Brown and D. Altermatt, *Acta Crystallogr., Sect. B.* , 1985, **41**, 244–247.

40 C. A. Rios Reyes, University of Wolverhampton, 2008.

41 L. N. Demianets, *Springer Berlin Heidelberg*, 1978, 97-123.

42 M. Y. Liu, W. S. You, Z. B. Lei, T. Takata, K. Domen and C. Li, *Chinese J. Catal.*, 2006, **27**, 556-558.

43 H. Li, E. M. Langer, P. Kegler and E. V. Alekseev, *Inorg. Chem.*, 2019, **58(15)**, 10333-10345.

44 C. A. Juillerat, V. V. Klepov, G. Morrison, K. A. Pace and H. C. Zur Loye, *Dalton Trans*, 2019, **48(10)**, 3162-3181.

45 G. Morrison and H.-C. zur Loye, *Cryst. Growth Des.*, 2016, **16(3)**, 1294-1299.

46 A. J. Lussier, R. A. K. Lopez and P. C. Burns, *Can. Mineral.*, 2016, **54**, 177-283.

47 A. L. Spek, *J. Appl. Crystallogr.*, 2003, **36**, 7-13.

48 C. L. Liu, H. K. Liu, W. J. Chang and K. H. Lii, *Inorg. Chem.*, 2015, **54(17)**, 8165-8167.

49 H. J. Li, P. Kegler, D. Bosbach and E. V. Alekseev, *Inorg. Chem.*, 2018, **57(8)**, 4745-4756.

50 Y. H. Chen, H. K. Liu, W. J. Chang, D. L. Tzou and K. H. Lii, *J. Solid State Chem.*, 2016, **236**, 55-60.

51 F. Liebau *Structural Chemistry of Silicates*; Springer-Verlag: Berlin, 1985.

52 G. Morrison, A. M. Latshaw, N. R. Spagnuolo and H. C. Zur Loye, *J. Am. Chem. Soc.*, 2017, **139(41)**, 14743-14748.

53 O. C. Gagne and F. C. Hawthorne, *Acta Cryst.* , 2016, **B72**, 602-625.

54 S. Surble, S. Obbade, S. Saad, S. Yagoubi, C. Dion and F. Abraham, *J. Solid State Chem.*, 2006, **179(10)**, 3238-3251.

55 E. V. Alekseev, S. V. Krivovichev, W. Depmeier, T. Malcherek, E. V. Suleimanovl and E. V. Chuprunov, *Zeitschrift Fur Kristallographie*, 2007, **222(8)**, 391-395.

56 F. D. Bo, S. M. Aksenov and P. C. Burns, *Z. Kristallogr.*, 2019, **234(6)**, 383-393.

57 J. P. J. Legros, Y. P. , *Acta. Cryst.* , 1975, **B31**, 1133-1139.

58 D. L. Rousseau, R. P. Bauman and S. P. S. Porto, *J. Raman Spectrosc.*, 1981, **10(Jan)**, 253-290.

59 S. N. Achary, D. Errandonea, D. Santamaria-Perez, O. Gomis, S. J. Patwe, F. J. Manjon, P. R. Hernandez, A. Munoz and A. K. Tyagi, *Inorg. Chem.*, 2015, **54(13)**, 6594-6605.

60 M. Gabelicarobert and P. Tarte, *Spectrochim Acta A*, 1979, **35(6)**, 649-654.

61 H. J. Li, P. Kegler, D. Bosbach and E. V. Alekseev, *Inorg. Chem.*, 2018, **57(8)**, 4745-4756.

62 I. I. Leonidov, V. P. Petrov, V. A. Chernyshev, A. E. Nikiforov, E. G. Vovkotrub, A. P. Tyutyunnik and V. G. Zubkov, *J. Phys. Chem. C*, 2014, **118(15)**, 8090-8101.

63 R. L. Frost and P. A. Williams, *Spectrochimica Acta Part a-Molecular and Biomolecular Spectroscopy*, 2004, **60(8-9)**, 2071-2077.

64 I. D. Zakir'yanova and P. A. Arkhipov, *Russ. Metall.*, 2017**(2)**, 86-90.

65 R. L. Frost, J. Cejka, M. L. Weier and W. Martens, *J. Raman Spectrosc.*, 2006, **37(4)**, 538-551.

66 E. P. Plesko, B. E. Scheetz and W. B. White, *Am. Mineral.*, 1992, **77(3-4)**, 431-437.

67 B. Xiao, H. Schlenz, J. Dellen, D. Bosbach, E. V. Suleimanov and E. V. Alekseev, *Cryst. Growth Des.*, 2015, **15(8)**, 3775-3784.

68 G. S. Henderson and R. T. Amos, *J. Non-Cryst. Solids*, 2003, **328(1-3)**, 1-19.

69 L. Y. Zhang, H. Li and L. L. Hu, *J. Alloys Compd.*, 2017, **698**, 103-113.

70 J. R. Bartlett and R. P. Cooney, *J. Mol. Struct.*, 1989, **193**, 295-300.

71 B. Xiao, P. Kegler, D. Bosbach and E. V. Alekseev, *Dalton Trans.*, 2016, **45(38)**, 15225-15235.

72 M. T. Paquesledent, *Spectrochim. Acta A*, 1976, **32(2)**, 383-395.

73 F. D. Bo, S. M. Aksenov and P. C. Burns, *J. Solid State Chem.*, 2019, **271**, 126-134.

Table 1. Crystallographic data of $K_8BrF(UO_2)_3(Ge_2O_7)_2$, $Rb_6(UO_2)_3(Ge_2O_7)_2{\cdot}0.5H_2O$, $Cs_6(UO_2)_2Ge_8O_{21}$, and $\boldsymbol{A}^+_2(UO_2)_3(GeO_4)_2$ ($\boldsymbol{A}^+$= Rb^+, Cs^+).

Compounds	$K_8BrF(UO_2)_3(Ge_2O_7)_2$	$Rb_6(UO_2)_3(Ge_2O_7)_2{\cdot}0.5H_2O$	$Cs_6(UO_2)_2Ge_8O_{21}$	$Rb_2(UO_2)_3(GeO_4)_2$	$Cs_2(UO_2)_3(GeO_4)_2$
fw (g/mol)	1736.16	1845.27	2254.24	1254.21	1349.09
Space group	***P*** -1	***P***-1	***P***-1	***P***nma	***P***nma
a/Å	7.3647(3)	7.4797(4)	7.4500(3)	10.2880(4)	10.60811(17)
b/Å	9.7768(6)	9.9013(6)	7.8701(3)	7.6612(2)	7.66072(12)
c/Å	9.9186(5)	10.1327(7)	14.7132(6)	16.1444(5)	16.1437(3)
α (deg)	70.779(5)	70.179(6)	91.077(3)	90.00	90.00
β (deg)	89.613(4)	89.046(5)	96.005(3)	90.00	90.00
γ (deg)	87.291(4)	86.240(5)	117.601(4)	90.00	90.00
Volume/$Å^3$	673.58(6)	704.43(8)	758.08(5)	1272.46(7)	1311.93(4)
Z	1	1	1	4	4
λ (Å)	0.71073	0.71073	0.71073	0.71073	0.71073
F (000)	760.0	790.0	970.0	2104.0	2248.0
ρ/g·cm^{-3}	4.280	4.350	4.938	6.547	6.830
GoF	1.074	0.927	1.021	1.015	1.085
R(F) for $F0^2$> $2\sigma(F0^2)$[a]	0.0757	0.0591	0.0348	0.0189	0.0186
wR2 ($F0^2$)[b]	0.2193	0.1383	0.0816	0.0374	0.0458

[a] $R(F) = \Sigma||F^0| - |F^c||/\Sigma|F^0|$ [b] $R(F_0^2) = [w(F_0^2 - F_c^2)2/\Sigma w(F_0^4)^{1/2}$

Table 2. Synthetic methods, structural classification, and U=O/U−O bond lengths of all reported uranyl germanates

No.	Compounds	Synthetic methods	U/Ge ratio	Uranyl units	Germanate units	SBU Types	U=O bond length (Å)	U-O bond length (Å)
1	$Cs_6(UO_2)_2Ge_8O_{21}$	HT	0.25	0-D (4-d)	2-D layer (4-d,5-d)	$4^2.5^2$-A2,5^4-A2	1.824	2.217-2.263
2	$K_6(UO_2)_3Ge_8O_{22}$[2]	HT	0.375	0-D (4-d)	0-D Ge_8O_{22} cluster	A, A2	1.830-1.832	2.213-2.259
3	$(Cu(H_2O)_4)((UO_2)(HGeO_4))_2(H_2O)_2$[57]	Hydrothermal	0.5	1-D chain (5-d)	0-D GeO_4	D	1.734-1.782	2.246-2.440
4	$Cs_2[(UO_2)(Ge_2O_6)](H_2O)$ [20]	Hydrothermal	0.5	0-D (4-d)	0-D Ge_4O_{12}square	A,A1,A2	1.809-1.828	2.203-2.265
5	β-$Cs_2(UO_2)Ge_2O_6$[2]	HT	0.5	0-D (4-d)	0-D Ge_4O_{12} square	A, A1,A2	1.792-1.829	2.219-2.242
6	α-$Cs_2(UO_2)Ge_2O_6$[2]	HT	0.5	0-D (4-d)	0-D Ge_4O_{12} square	A1	1.823-1.843	2.185-2.289
7	$K_8BrF(UO_2)_3(Ge_2O_7)_2$	HT	0.75	0-D (4-d)	0-D Ge_2O_7	A, A2	1.807-1.839	2.210-2.267
8	$[KK_6Cl][(UO_2)_3(Ge_2O_7)_2]$[3]	HT	0.75	0-D (4-d)	0-D Ge_2O_7	A, A1	1.827-1.836	2.208-2.268
9	$[KK_6Br_{0.6}F_{0.4}][(UO_2)_3(Ge_2O_7)_2]$[3]	HT	0.75	0-D (4-d)	0-D Ge_2O_7	A, A1	1.825-1.840	2.207-2.272
10	$Rb_6(UO_2)_3(Ge_2O_7)_2{\cdot}0.5H_2O$	Hydrothermal	0.75	0-D (4-d)	0-D Ge_2O_7	A, A2	1.795-1.806	2.197-2.250
11	$K_4Na_2(UO_2)_3(Ge_2O_7)_2{\cdot}3H_2O$[49]	Hydrothermal	0.75	0-D (4-d)	0-D Ge_2O_7	A, A2	1.833- 1.843	2.227- 2.241
12	$NaK_6Cl(UO_2)_3(Ge_2O_7)_2$[2]	HT	0.75	0-D (4-d)	0-D Ge_2O_7	A, A1	1.810-1.841	2.201-2.265
13	$[K_{0.6}Na_{0.4}K_5CsCl_{0.5}F_{0.5}][(UO_2)_3(Ge_2O_7)_2]$[3]	HT	0.75	0-D (4-d)	0-D Ge_2O_7	A, A1	1.809-1.832	2.199-2.262
14	$[K_{0.8}Na_{0.2}K_{4.8}Cs_{1.2}Cl_{0.5}F_{0.5}][(UO_2)_3(Ge_2O_7)_2]$[3]	HT	0.75	0-D (4-d)	0-D Ge_2O_7	A, A1	1.781-1.856	2.178-2.298
15	$Cs_6((UO_2)_3(Ge_2O_7)_2)(H_2O)_4$[22]	HT/HP hydrothermal	0.75	0-D (4-d)	0-D Ge_2O_7	A, A1	1.831-1.837	2.195-2.241
16	$[Na_{0.9}Rb_{6.1}F][(UO_2)_3(Ge_2O_7)_2]$[3]	HT	0.75	0-D (4-d)	0-D Ge_2O_7	A, A1	1.830-1.848	2.209-2.252
17	$[KK_{1.8}Cs_{4.2}F][(UO_2)_3(Ge_2O_7)_2]$[3]	HT	0.75	0-D (4-d)	0-D Ge_2O_7	A, A1	1.827-1.842	2.205-2.257
18	$[Cs_6K_{1.9}Ag_{0.1}Cl_2][(UO_2)_3(Ge_2O_7)_2]$[3]	HT	0.75	0-D (4-d)	0-D Ge_2O_7	A, A1	1.828-1.854	2.216-2.252
19	$Na_2Cs_6Cl_2(UO_2)_3(Ge_2O_7)_2$[2]	HT	0.75	0-D (4-d)	0-D Ge_2O_7	A, A1	1.829-1.834	2.213-2.252

20	$[Cs_6K_2Cl_2][(UO_2)_3(Ge_2O_7)_2]$[3]	HT	0.75	0-D (4-d)	0-D Ge_2O_7	A, A1	1.831-1.844	2.207-2.253
21	$[Cs_6Ag_{0.3}Na_{1.7}Cl_2][(UO_2)_3(Ge_2O_7)_2]$[3]	HT	0.75	0-D (4-d)	0-D Ge_2O_7	A, A1	1.830-1.841	2.217-2.244
22	$[Cs_2Cs_5F][(UO_2)_3(Ge_2O_7)_2]$[3]	HT	0.75	0-D (4-d)	0-D Ge_2O_7	A, A1	1.822-1.842	2.175-2.239
23	$[Cs_6Cs_{0.71}Cl_{0.71}][(UO_2)_3(Ge_2O_7)_2]$[3]	HT	0.75	0-D (4-d)	0-D Ge_2O_7	A, A1	1.860	2.179-2.291
24	$[Cs_6Ag_{0.4}Na_{1.6}Cl_2][(UO_2)_3(Ge_2O_7)_2]$[3]	HT	0.75	0-D (4-d)	0-D Ge_2O_7	A, A1	1.835-1.839	2.213-2.248
25	$[Cs_6Ag_2Cl_2][(UO_2)_3(Ge_2O_7)_2]$[3]	HT	0.75	0-D (4-d)	0-D Ge_2O_7	A, A1	1.840-1.859	2.203-2.241
26	$Mg[(UO_2)_2(Ge_2O_6(OH)_2)](H_2O)_{4.4}$[56]	Hydrothermal (200 °C)	1	2-D (5-d)	0-D Ge_2O_8H	E	1.719	2.258-2.403
27	$Rb(UO_2)(HGeO_4)\cdot H_2O$[43]	Hydrothermal	1	1-D chain (5-d)	0-D GeO_4	D	1.778-1.791	2.304-2.494
28	$K_2(UO_2)GeO_4$[2]	HT	1	0-D (4-d)	0-D GeO_4	A	1.82	2.247
29	$K_4[(UO_2)_8(HGe_2O_7)_4](H_2O)_2$[73]	Hydrothermal	1	1-D chain (5-d)	0-D Ge_2O_7	D	1.725-1.776	2.278-2.379
30	$Co_2[(UO_2)_8(HGe_2O_7)_4](H_2O)_6$[73]	Hydrothermal	1	1-D chain (5-d)	0-D Ge_2O_7	D	1.762-1.786	2.307-2.460
31	$Cs(UO_2)(HGeO_4)\cdot H_2O$[43]	Hydrothermal	1	1-D chain (5-d)	0-D GeO_4	D	1.783-1.785	2.289-2.482
32	$H_3O(UO_2)_2(HGe_2O_7)\cdot 2H_2O$[49]	Hydrothermal	1	1-D chain (5-d)	0-D Ge_2O_7	D	1.766-1.767	2.298-2.464
33	$Na_2(UO_2)GeO_4$[49]	HT and Hydrothermal	1	0-D (4-d)	0-D GeO_4	A	1.823	2.252
34	$Ba_2[(UO_2)_8(HGe_2O_7)_4](H_2O)_3$[73]	Hydrothermal	1	1-D chain (5-d)	0-D Ge_2O_7	D	1.778-1.790	2.301-2.454
35	$Rb_4[(UO_2)_8(HGe_2O_7)_4](H_2O)_2$[73]	Hydrothermal	1	1-D chain (5-d)	0-D Ge_2O_7	D	1.736-1.783	2.317-2.455
36	$Cs_2(UO_2)GeO_4$[2]	HT	1	1-D chain (4-d)	0-D Ge_4O_{12} square	C	1.867	2.140-2.238
37	$Cs[(UO_2)_2(HGe_2O_7)]$[73]	Hydrothermal	1	1-D chain (5-d)	0-D Ge_2O_7	D	1.775-1.809	2.318-2.453
38	$Ag[(UO_2)_2(HGe_2O_7)](H_2O)$ [20]	Hydrothermal	1	1-D chain (5-d)	0-D Ge_2O_7	D	1.768-1.798	2.287-2.458
39	$Rb_2(UO_2)_3(GeO_4)_2$	HT/HP	1.5	1-D chain (5-d)	1-D chain(5-d)	E	1.792-1.815	2.276-2.594

40	$Ag_2[(UO_2)_3(GeO_4)_2](H_2O)_2$[20]	Hydrothermal	1.5	1-D column (5-d)	1-D chain(5-d)	E	1.797-1.810	2.283-2.586
41	$Cs_2(UO_2)_3(GeO_4)_2$	HT/HP	1.5	1-D chain (5-d)	1-D chain(5-d)	E	1.793-1.813	2.284-2.567
42	$(UO_2)_2(GeO_4)(H_2O)_2$[57]	Hydrothermal	2	1-D chain (5-d)	0-D GeO_4	D	1.771	2.310-2.438

(1) HT is High temperature method; HT/HP Hydrothermal is high temperature, high pressure hydrothermal method.
(2) 0-D, 1-D and 2-D are uranyl or germanate dimensionality. (3) 4-d, 5-d, and 6-d are four-, five- and six-coordinated uranyl/germanate polyhedra.

Table 3. Vibrational Modes of $K_8BrF(UO_2)_3(Ge_2O_7)_2$, $Rb_6(UO_2)_3(Ge_2O_7)_2{\cdot}0.5H_2O$, $Cs_6(UO_2)_2Ge_8O_{21}$, and $\boldsymbol{A}^+_2(UO_2)_3(GeO_4)_2$ ($\boldsymbol{A}^+$= Rb^+, Cs^+).

Compounds	Point group	Mechanical representation	Infrared active modes	Raman active modes
$K_8BrF(UO_2)_3(Ge_2O_7)_2$	C_i (-1)	$54A_g + 63A_u$	$60A_u$	$54A_g$
$Rb_6(UO_2)_3(Ge_2O_7)_2{\cdot}0.5H_2O$	C_i (-1)	$48A_g + 60A_u$	$57A_u$	$48A_g$
$Cs_6(UO_2)_2Ge_8O_{21}$	C_i (-1)	$63A_g + 69A_u$	$66A_u$	$63A_g$
$\boldsymbol{A}^+_2(UO_2)_3(GeO_4)_2$ ($\boldsymbol{A}^+$= Rb^+, Cs^+)	D_{2h} (mmm)	$37A_g + 26A_u + 26B_{1g} + 37B_{1u} + 37B_{2g} + 26B_{2u} + 26B_{3g} + 37B_{3u}$	$36B_{1u} + 25B_{2u} + 36B_{3u}$	$37A_g + 26B_{1g} + 37B_{2g} + 26B_{3g}$

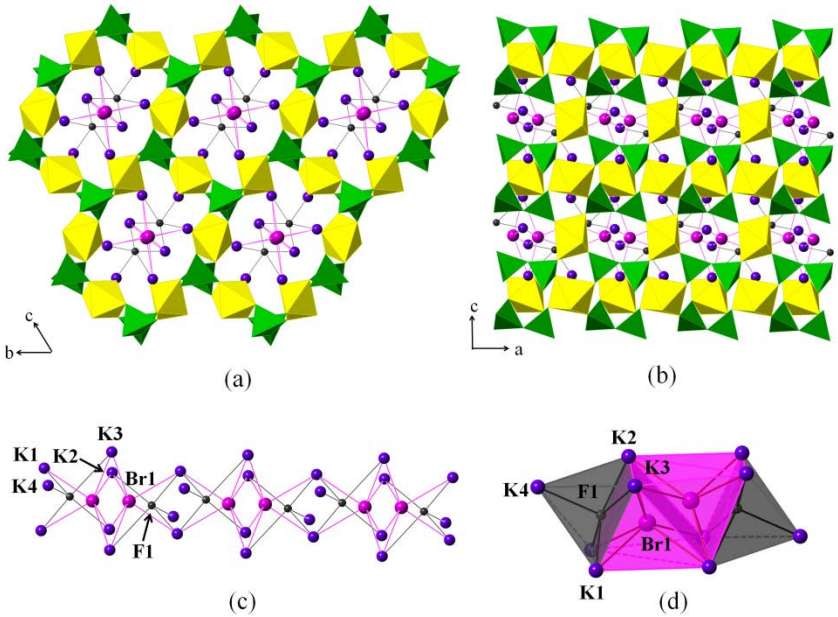

Figure 1. (a, b) Structure of $K_8BrF(UO_2)_3(Ge_2O_7)_2$projected along ***a*** and ***b*** axes. (c) Salt-inclusion $[K_8BrF]^{6+}$ units in the structure of $K_8BrF(UO_2)_3(Ge_2O_7)_2$ in atomic and polyhedral presentation (d). The yellow and green polyhedra are UO_6 and GeO_4, respectively.Mauve, magenta and black spheres are K cations, Br^- and F^- anions, respectively.

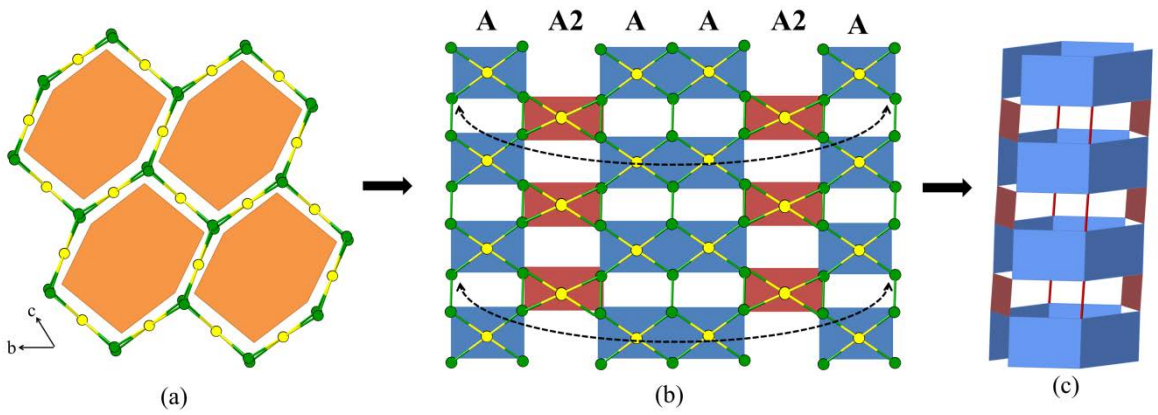

Figure 2. (a) Topology of $K_8BrF(UO_2)_3(Ge_2O_7)_2$ structure with 12-membered hexagon shaped channel along ***a*** axis. (b) The topology of the ideal unfolding wall of a 12-membered channel. Blue rectangles represent SBU [UGe_4] pentamers (**A**-type) and dark red rectangles represent SBU [UGe_4] pentamers (**A2**-type). (c) Ideal hexagonal prism constructed from two types of [UGe_4] pentamers.

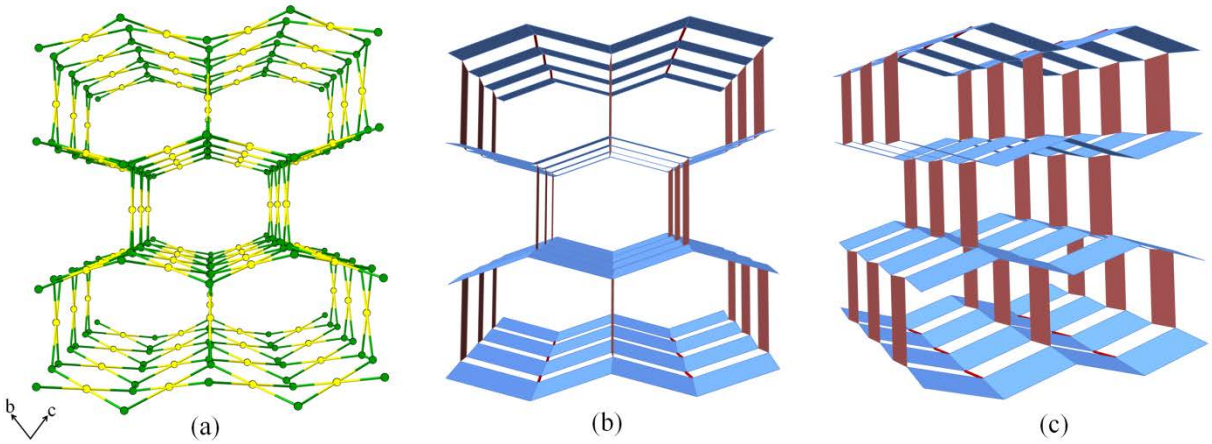

Figure 3. (a) Topology representation of $K_8BrF(UO_2)_3(Ge_2O_7)_2$ along ***a*** axis. (b,c) The idealized 3D schematic representation of $K_8BrF(UO_2)_3(Ge_2O_7)_2$ structure built upon $[UGe_4]$ pentamers (**A**-type) and (**A2**-type), highlighted by blue and dark red rectangles, respectively.

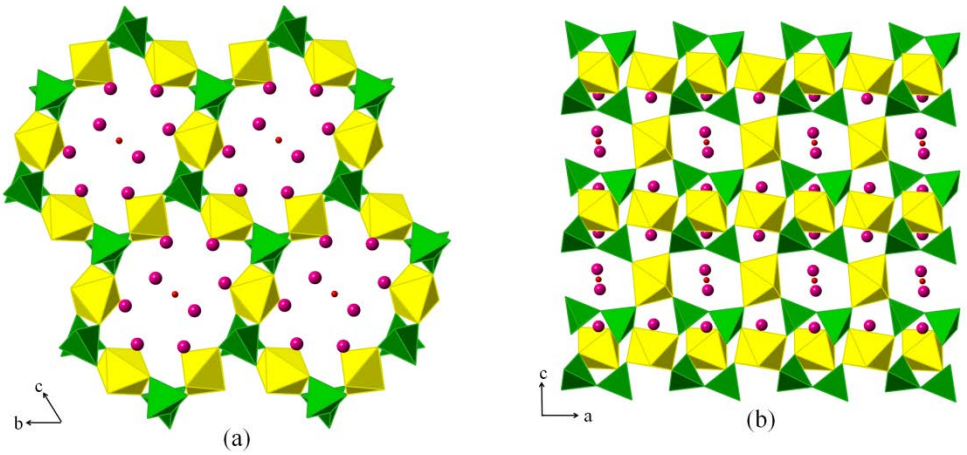

Figure 4. (a, b) Structure of $Rb_6(UO_2)_3(Ge_2O_7)_2 \cdot 0.5H_2O$compound projected along ***a*** and ***b*** axes. U and Ge polyhedra are yellow and green, respectively. Large purple and small red spheres are cesium cations and H_2O molecular, respectively.

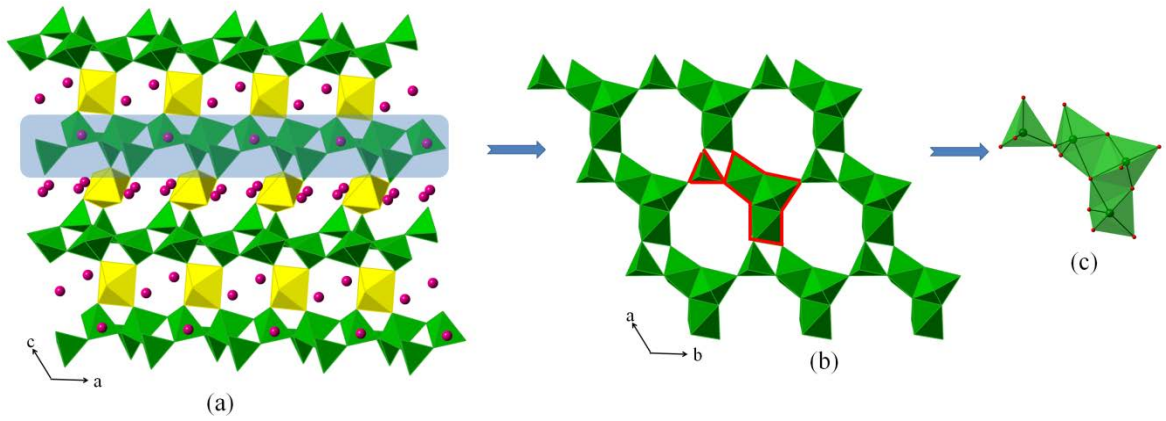

Figure 5. (a) Structure of $Cs_6(UO_2)_2Ge_8O_{21}$ along ***b*** axis. (b) A germanate sheet constructed by 4- and 5-coordinated Ge. (c) The basic unit of the germanate sheet. The yellow polyhedra are uranyl tetragonal bipyramids, green polyhedra are germanate tetrahedra and trigonal bipyramids, and dark pink spheres are cesium cations.

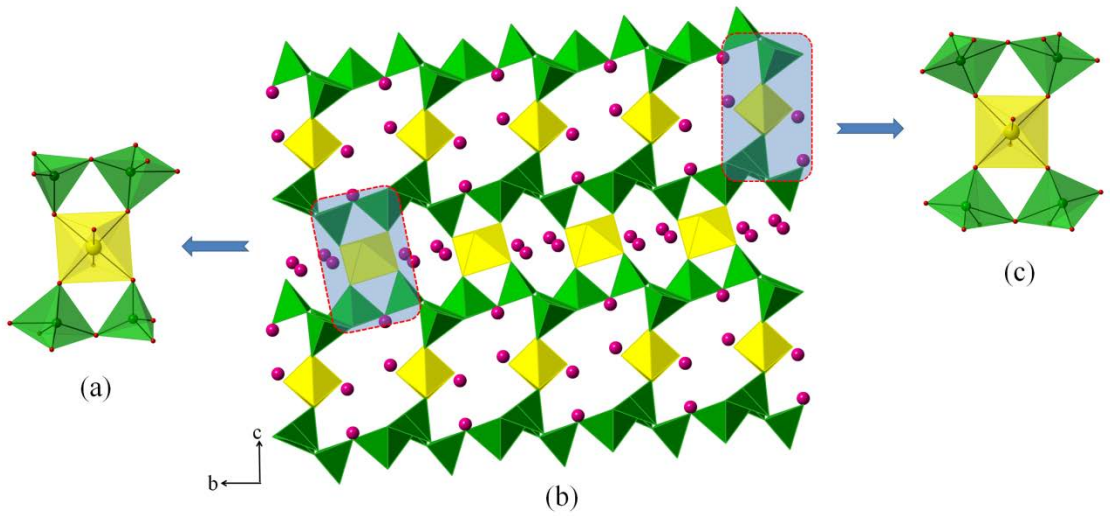

Figure 6. (a) SBUs of uranyl germanates: [UGe_4] pentamers (4- and 5-coordinated Ge) (**$4^2.5^2$-A2** type). (b) Structure of compound $Cs_6(UO_2)_2Ge_8O_{21}$ projected along a axis. (c) SBUs of uranyl germanates: [UGe_4] pentamers (5-coordinated Ge) (**5^4-A2** type). U and Ge polyhedra are yellow and green, respectively, and Cs atoms are dark pink.

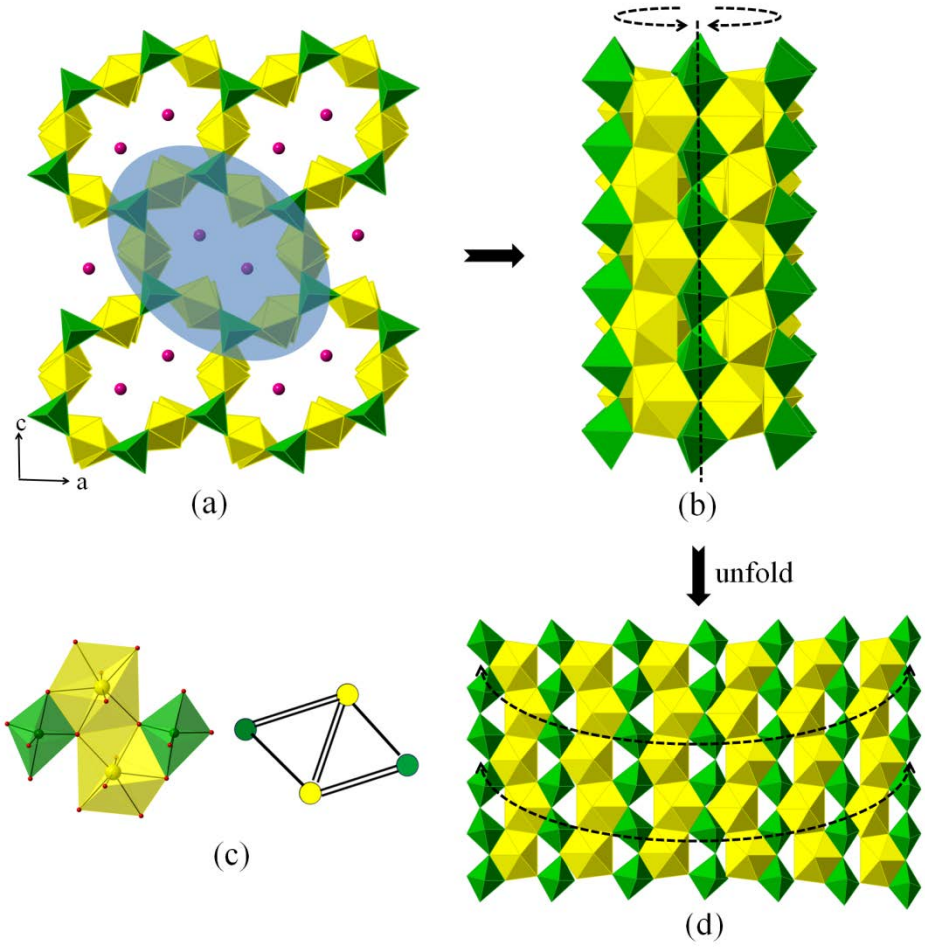

Figure 7. (a) Structure of $Cs_2(UO_2)_3(GeO_4)_2$ compound projected along ***b*** axis. (b) 12-membered channel in the structure of $Cs_2(UO_2)_3(GeO_4)_2$ containing 7-coordinated uranyl chains and 5-coordinated germanate chains. (c) Polyhedra representation and topology of SBUs $[U_2Ge_2]$ tetramers (7-coordinated U and 5-coordinated Ge) in the structure. (d) Unfolding polyhedra of 12-membered channel constructed by $[U_2Ge_2]$ tetramers. U and Ge polyhedra are yellow and green, respectively, and Cs atoms are dark pink.

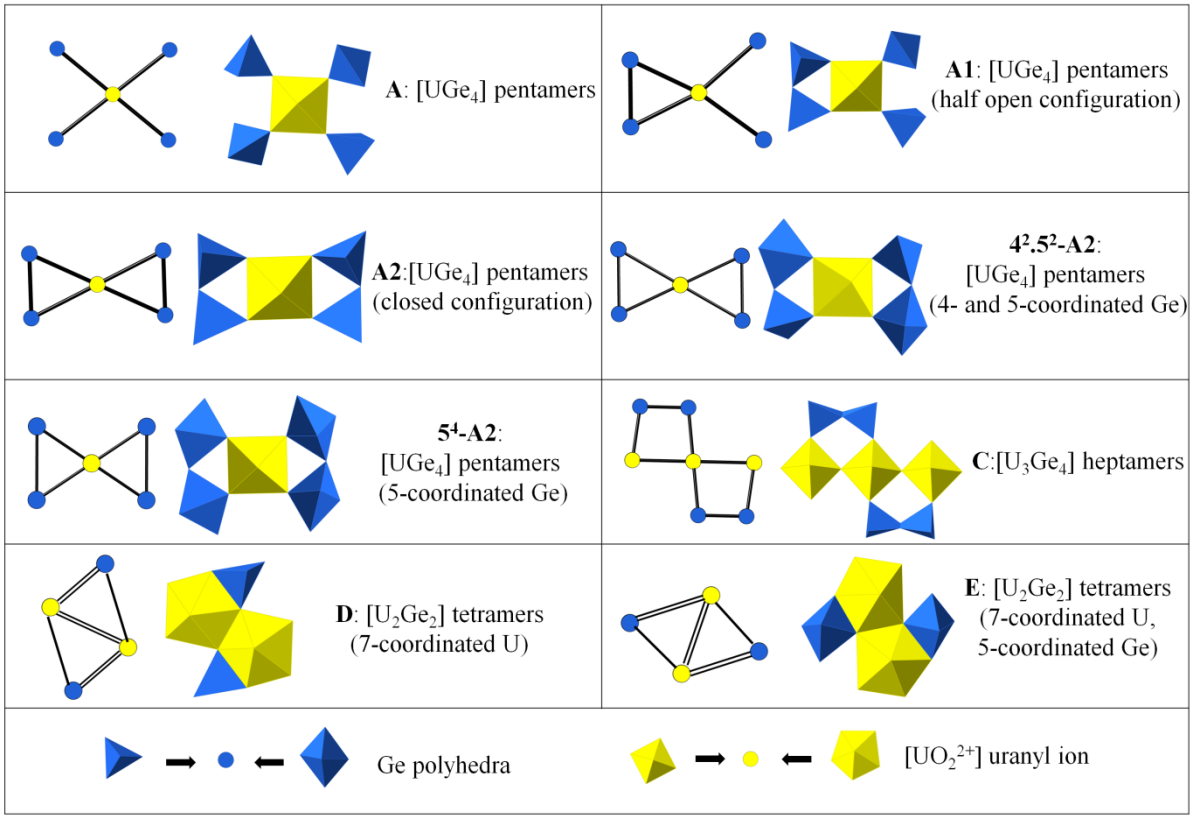

Figure 8. Polyhedral and ball-and-stick representations of the updated SBUs extracted from all reported uranyl germanate compounds without uranyl cation-cation interactions. U and Ge polyhedra are yellow and blue, respectively.

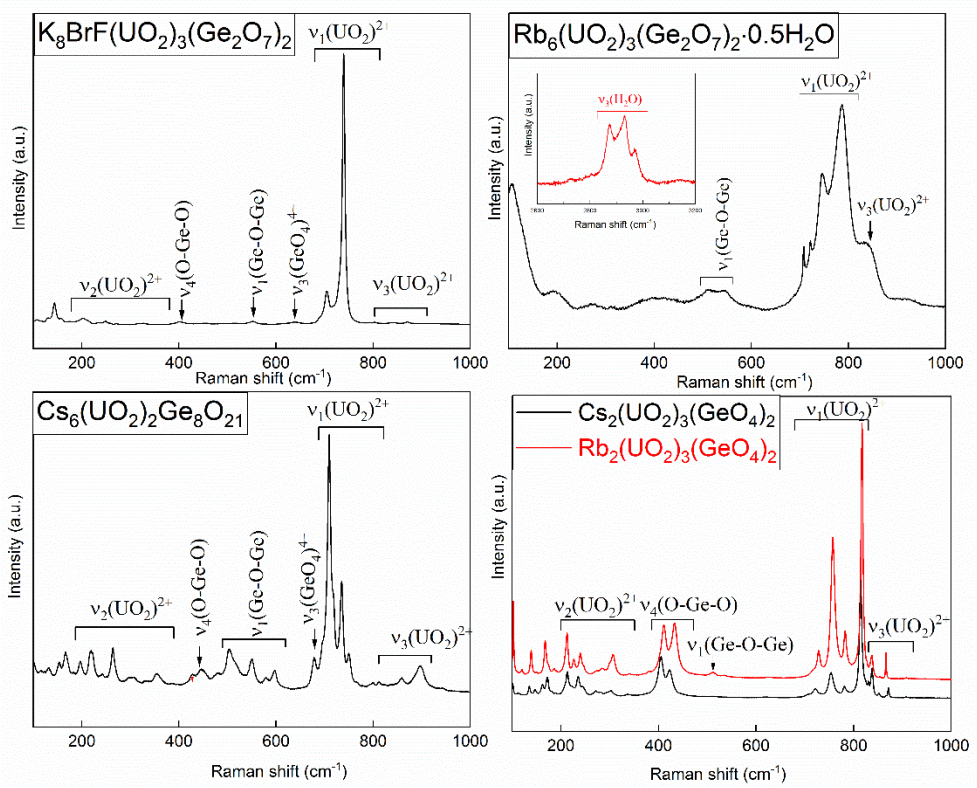

Figure 9. Raman spectra of $K_8BrF(UO_2)_3(Ge_2O_7)_2$, $Rb_6(UO_2)_3(Ge_2O_7)_2{\cdot}0.5H_2O$, $Cs_6(UO_2)_2Ge_8O_{21}$and $\boldsymbol{A}^+_2(UO_2)_3(GeO_4)_2$ ($\boldsymbol{A}^+$ = Rb, Cs)in the 100 − 1000 cm^{-1} region, and Raman spectrum of $Rb_6(UO_2)_3(Ge_2O_7)_2{\cdot}0.5H_2O$ in the 2600 − 3200 cm^{-1} region.